Research article

Hybrid nonlinear regression model versus MARS, MEP, and ANN to evaluate the effect of the size and content of waste tire rubber on the compressive strength of concrete

Dilshad Kakasor Ismael Jaf [a,*], Aso Abdalla [b], Ahmed Salih Mohammed [b], Payam Ismael Abdulrahman [c,**], Rawaz Kurda [d,e,f], Azad A. Mohammed [b]

[a] Civil Engineering Department, College of Engineering, Salahaddin University-Erbil, Kurdistan, Iraq
[b] Civil Engineering Department, College of Engineering, University of Sulaimani, Kurdistan, Iraq
[c] Scientific Research Centre, Soran University, Soran, Kurdistan Region, Iraq
[d] Department of Highway and Bridge Engineering, Technical Engineering College, Erbil Polytechnic University, Erbil, 44001, Iraq
[e] Department of Civil Engineering, College of Engineering, Nawroz University, Duhok, 42001, Iraq
[f] CERIS, Civil Engineering, Architecture and Georresources Department, Instituto Superior Técnico, Universidade de Lisboa, Av. Rovisco Pais, 1049-001, Lisbon, Portugal

ARTICLE INFO

ABSTRACT

Tire rubber waste is globally accumulated every year. Therefore, a solution to this problem should be found since, if landfilled, it is not biodegradable and causes environmental issues. One of the most effective ways is recycling those wastes or using them as a replacement for normal aggregate in the concrete mixture, which has high impact resistance and toughness; thus, it will be a good choice. In this study, 135 data were collected from previous literature to develop a model for the prediction of rubberized concrete compressive strength; the database comprised different mixture proportions, the maximum size of the rubber (1–40 mm), and the rubber percentage (0–100%) replacing natural fine and coarse aggregates were among the input parameters in addition to cement content (380–500 kg/m^3) water content (129–228 kg/m^3), fine aggregate content (0–925 kg/m^3), coarse aggregate content (0–1303 kg/m^3), and curing time of the samples (1–96 Days); then the collected data were used in developing Multi Expression Programming (MEP), Artificial Neural Network (ANN), Multi Adaptive Regression Spline (MARS), and Nonlinear Regression (NLR) Models for predicting compressive strength (CS) of rubberized concrete. The parametric analysis reveals that as the maximum rubber size increases, the reduction in compressive strength becomes more pronounced. Notably, this strength decline is more significant when rubber replaces coarse aggregate than its replacement of fine aggregate. Among the input parameters considered, it is evident that the fine aggregate content exerts the most substantial influence on the compressive strength of rubberized concrete. Its impact on predicting compressive strength surpasses other factors, with the concrete samples' curing time ranking second in importance. According to the assessment tools, the ANN model performed better than other developed models, with high R^2 and lower RMSE, MAE, SI, and MAPE. Additionally, ANN and MARS models

* Corresponding author.
** Corresponding author.
E-mail addresses: dilshad.jaf@su.edu.krd (D.K. Ismael Jaf), aso.abdalla@univsul.edu.iq (A. Abdalla), ahmed.mohammed@univsul.edu.iq (A.S. Mohammed), Payam@soran.edu.iq, payam.abdulrahman@soran.edu.iq (P.I. Abdulrahman), Rawaz.Kurda@tecnico.ulisboa.pt (Rawaz Kurda), Azad.mohammed@univsul.edu.iq (A.A. Mohammed).

predicted the CS of different sizes better than MEP and NLR models. Subsequently, we employed the collected data to develop predictive models using Multi Expression Programming (MEP), Artificial Neural Network (ANN), Multi Adaptive Regression Spline (MARS), and Nonlinear Regression (NLR) techniques to forecast the compressive strength (CS) of rubberized concrete. The statistical analysis tools assessed the performance of these developed models through various evaluation criteria, including the Coefficient of Determination (R^2), Root Mean Square Error (RMSE), Mean Absolute Error (MAE), Scatter Index (SI), and Mean Absolute Percentage Error (MAPE). In summary, our study underscores the efficacy of recycling rubber materials in concrete production. It presents a powerful predictive model for assessing the compressive strength of rubberized concrete, with the ANN model standing out as the most accurate and reliable choice for this purpose.

1. Introduction

The handling of waste products is among the most significant environmental problems worldwide. Stockpiles of recycled industrial wastes have become a big problem because the waste tire is not biodegradable even after long-term landfill application. Reusing tire rubber as a replacement for coarse and fine aggregate in concrete is a good option for discarding excess waste tire rubber [1–3]. When desired properties need to be improved in plain concrete, such as low density, high toughness, sound insulation, and high energy absorption, some materials may be used; waste tire rubber is one of them [4].

Once natural aggregate in concrete is replaced with waste tire rubber, physical and mechanical properties will be extremely affected. Different research works have been conducted to evaluate the mechanical performance of rubberized concrete. Eldin and Senouci [1] evaluated some physical and engineering properties of rubberized concrete. In the study, naturally coarse and fine aggregates were replaced with up to 100% tire chips and crumb rubber as a percentage by aggregate volume; test results indicated that the concrete showed a ductile and plastic failure rather than a brittle failure. It was also concluded that the rubberized concrete has adequate workability. A study was performed by Güneyisi et al. [2] to obtain information about the effect of using silica fume on the mechanical characteristics of rubberized concrete. 2.5–50% of the natural aggregate (by volume) was replaced with rubber, and 5–20% of cement was replaced with silica fume. Results displayed when silica fume was added to rubberize the mechanical properties were enhanced through improved matrix strength. Also, replacing up to 25% of the aggregate showed adequate strength from 16 to over 30 MPa.

Crumb rubber particles have low density and lower elastic modulus, affecting the compressive, splitting, and flexural tensile strengths. These properties were decreased by 84, 51, and 72% when the replacement ratio exceeded 30% [5]. Grinys et al. [5] concluded that Adding a small amount of crumb rubber increased the splitting tensile strength, and the decrease in splitting tensile strength was lower than that of compressive strength by 61%. Ismail et al. [6] tested rubberized concrete with fly ash, slag, and metakaolin as supplementary cementitious materials. The compressive, flexural, and splitting tensile strength of the modified rubberized concrete were evaluated. The results revealed that the metakaolin improved the mixture stability and facilitated the development of concrete with low density (2100 kg/m^3) and a suitable stability-to-strength ratio with up to 30% crumb rubber.

Five different concrete mixtures were created, and we cast concrete cubes, cylinders, and prisms using extracts from waste tires. To prepare the crumb rubber, we soaked it in sodium hydroxide and then replaced a portion of the fine aggregates in the concrete mixture, specifically at 10% and 30%. Also added, steel fibers were extracted at 1% and 2% per volume for each mixture. After subjecting the specimens to regular curing and various drying conditions, we conducted tests to assess their compressive strength, indirect splitting tensile strength, flexural strength, and air permeability. We developed a portable apparatus for measuring air permeability.

In cases where we replaced 10% of the fine aggregate with crumb rubber and added 1% steel fibers, we found that the splitting tensile strength and flexural strength were 21% and 22.6% higher, respectively, than those of the control mix. Furthermore, when these specimens were exposed to oven drying at 105 °C for 12 h, their compressive strength increased by 17% compared to the control specimens subjected to the same conditions. However, the splitting tensile and flexural strength decreased after exposure to elevated temperatures. The introduction of crumb rubber and steel fibers as partial replacements for fine aggregate had varying effects on the air permeability of the concrete, depending on the percentages used. Notably, the oven-drying curing method improved permeability, as indicated by a 15% increase in the permeability time index of specimens containing 10% crumb rubber and 1% steel fibers compared to air-dried samples. This study supports waste tire extracts as a viable and environmentally friendly solution for partially replacing fine aggregate in concrete, suitable for indoor and outdoor applications. Additionally, it demonstrates this method's economic and ecologically conscious potential in reducing carbon emissions [6].

Tire rubber can significantly impact various properties of concrete when used as a partial replacement for traditional aggregates. Here are some ways in which tire rubber affects concrete properties:

Compressive Strength: Incorporating tire rubber in concrete typically leads to a reduction in compressive strength. This is because rubber is less dense and less rigid than traditional aggregates. The extent of the strength reduction depends on factors such as rubber particle size and content.

The presence of rubber can also lower the flexural strength of concrete. However, this reduction can be mitigated by optimizing the rubber content and distribution within the concrete mixture.

Rubber particles can act as internal lubricants within the concrete mix, improving workability and making it easier to handle and place. This can be particularly beneficial in specific construction applications. Rubber is less dense than traditional aggregates, so

incorporating it into concrete can reduce the overall density of the concrete. This can be advantageous in applications where lower weight is desired, such as in lightweight concrete. Rubber has insulating properties, so rubberized concrete can offer improved thermal insulation compared to conventional concrete. This can benefit construction projects where energy efficiency and temperature control are important. Rubberized concrete can provide better sound absorption properties due to the inherent sound-dampening characteristics of rubber. This can be valuable in projects aimed at reducing noise pollution. Rubberized concrete can exhibit improved resistance to cracking and spalling, especially in freeze-thaw cycles, thanks to the flexibility of rubber particles. This can enhance the durability of structures made with rubberized concrete. Incorporating recycled tire rubber into concrete reduces the environmental impact by recycling waste materials and lessening the demand for traditional aggregates. It can also contribute to sustainability and green building practices. Using tire rubber in concrete can lower the carbon footprint of construction projects by reducing the need for energy-intensive processes to produce traditional aggregates. Cost Considerations: While rubberized concrete can offer numerous benefits, it's essential to consider the cost implications. Tire rubber may be more expensive than traditional aggregates, and special processing may be required. In summary, the use of tire rubber in concrete can influence various properties, and the extent of these effects depends on factors such as rubber content, particle size, and the specific application. Proper mix design and testing are essential to optimize the balance between desirable properties and potential drawbacks when using rubberized concrete [6–10]. This review focuses on the influence of rubber content and particle size on various properties of concrete, including unit weight, slump, entrapped air, compressive strength, splitting tensile strength, modulus of rupture, modulus of elasticity, ultimate strain, viscous damping ratio. The findings of this review indicate that researchers have replaced fine and coarse aggregates with rubber in different proportions, ranging from 5% to 100% by volume. As a result of these replacements, the concrete exhibited a wide range of strength losses, varying from 0.0% to as high as 85%. These losses depended on factors such as the size of the rubber particles and the rubber content used in the mixture. Additionally, the review highlights the positive impact of chemical treatments applied to the rubber before its incorporation into the concrete, which significantly improved the mechanical properties of the resulting concrete. Notably, increasing the rubber content in the concrete led to increased flexibility and viscous damping ratio compared to conventional concrete. In particular, rubberized concrete demonstrated an ultimate strain and viscous damping ratio of 16% and 120% higher than traditional concrete. This review underscores the multifaceted effects of rubber content and size on various concrete properties, highlighting the potential for enhancing ductility and damping characteristics in rubberized concrete compared to traditional concrete mixes [11]. Soft computing models published related to rubberized concrete computing models, including artificial neural networks (ANNs), genetic algorithms, fuzzy logic, and other machine learning techniques, have been applied to various aspects of rubberized concrete research. It can use specific search terms and explore academic databases to find similar soft computing models related to rubberized concrete. Here are some potential areas and keywords to consider: Compressive Strength Prediction: Search for soft computing models that predict the compressive strength of rubberized concrete. Keywords could include "compressive strength prediction," "ANN for concrete strength," or "fuzzy logic model for rubberized concrete." Optimization of Mix Proportions: Look for studies that use soft computing techniques to optimize the mix proportions of rubberized concrete for specific performance criteria, such as strength, workability, or cost-effectiveness. Keywords might include "genetic algorithm optimization," "mix design using soft computing," or "fuzzy-based mix proportion optimization." Durability Assessment: Explore research on soft computing models that assess the durability of rubberized concrete under various environmental conditions. Keywords could include "fuzzy logic durability assessment," "ANN for concrete durability," or "genetic algorithm and rubberized concrete durability." Material Properties Estimation: Investigate models that use soft computing techniques to estimate material properties of rubberized concrete, such as elastic modulus, permeability, or porosity. Keywords might include "fuzzy logic material property estimation," "ANN for concrete porosity," or "soft computing and rubberized concrete properties." Numerical Simulations: Explore soft computing-based numerical simulations or finite element analysis (FEA) models used to simulate the behavior of rubberized concrete structures [12–14]. Different modeling techniques were used in the literature to predict the compressive strength of rubberized concrete. Kovačević et al. [7] summarized the modeling approaches used in the literature in the model developments, including ANN, fuzzy logic, random forest, k-nearest neighbor (KNN), gene expression programming (GEP), Gaussian process regression, supporting vector machine learning (SVM), regression tree, and random forested algorithm based on beetle antenna search. These models yielded good results and different performances. Some machine learning models are difficult to present, and simpler models could not be developed through their training. As a result, in the current study, in addition to ANN, Multi-Expression Programming (MEP), Multi-Adaptive Regression Spline (MARS), and Nonlinear Regression (NLR) models were used to predict the compressive strength of rubberized concrete.

The current study aims to develop predictive models to estimate compressive, flexural, and splitting tensile strengths and find the relation between rubberized concrete's compressive strength and tensile strength. The following are the main objectives.

    i. Modeling the effect of rubber content, w/c, and curing time on the mechanical properties of rubberized concrete.
   ii. Developing models to estimate the compressive of rubberized concrete
  iii. Predicting the impact of maximum rubber size on the CS of rubberized concrete.
  iv. Finding the efficiency of the proposed model in predicting the compressive strength of different sample sizes.
   v. Finding the most influential parameter on prediction of rubberized concrete compressive strength.

2. Materials and methods

Fig. 1 shows the flowchart diagram of the current study, including the steps followed to export the best-developed models. The process comprises (i) data collection, (ii) data presentation and analysis, (iii) data splitting, (iv) model development, (v) evaluations and comparison between models, and finally (vi) sensitivity analysis.

2.1. Data collection

In the current study, 135 datasets were collected from previous literature to develop analytical models to estimate the compressive strength of rubberized concrete. Cement content (C, kg/m^3), water content (W, kg/m^3), superplasticizer content (SP, kg/m^3), coarse aggregate (CA, kg/m^3), fine aggregate content (FA, kg/m^3), rubber content (R, % by volume of aggregate), maximum rubber size (MRS, mm), and curing time (t, Days) were considered as input parameters (Predictors) and the compressive strength was the only target of the developed models. The summary of collected datasets is displayed in Table 1. Moreover, The collected data were statistically analyzed using mean, standard deviation (SD), variance (Var), kurtosis (Kur), and skewness (Skew); the result of the statistical analysis is shown in Table 2. The relationship between CS and the predictors is shown in Fig. 2, which presents a scatter plot with a marginal histogram of each parameter. Finally, Fig. 3 shows the histogram of compressive strength of rubberized concrete mixtures from 1 to 96 days of curing with a mean of 35.4 MPa, SD of 20.1 MPa, Var of 405.6, Kur of −0.868, and Skew of 0.074.

2.2. Modeling

A correlation matrix was drawn to determine the correlation between compressive strength and the predictors to show if there is a possible high correlation between them and predict the compressive strength using only one parameter. As shown in Fig. 4, the correlation between compressive strength and the input parameters is not as high as possible to be used to predict the compressive strength; therefore, in the following subsections, the modeling approaches used in the current study are explained.

2.2.1. Multi-expression programming (MEP)

The genetic algorithm (GA), which Holland introduced in the early 1970s [8], was extended to GP, and it was mainly proposed by
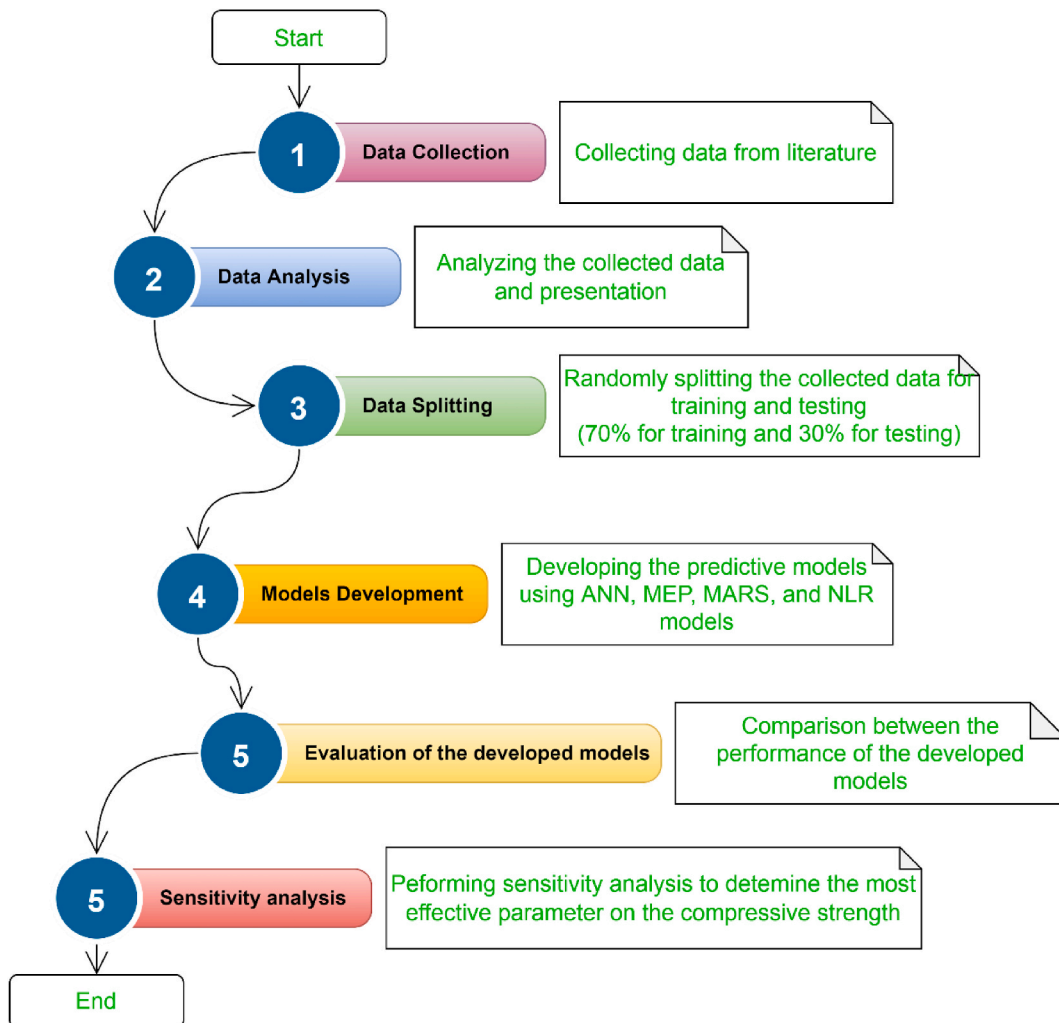
Fig. 1. Flowchart of the current study methodology.

Table 1
Summary of collected data for rubberized concrete.

Reference	No. of Data	C (kg/m³)	W (kg/m³)	SP (kg/m³)	FA (kg/m³)	CA (kg/m³)	R (%)	MRS (mm)	t (Days)	CS (MPa)
[1]	20	446	214	0	0–608	0–1094	0–100	6.35 and 40	7 and 28	5–34
[2]	14	450	180	13.5	635–688	980–1062	0–50	4	28	7–76
[5]	14	451	160	2.255	700–875	949	0–30	1, 2, and 3	28	10–64
[23]	10	425	191	0	498–575	1202	0–20	4.75	7 and 28	15–36.2
[6]	14	550	220	1.06–2.63	678–925	648	0–40	4.75	7 and 28	19–54
[24]	6	380	129	0	796–865	1010	0–25	9.5	28	36–55
[25]	27	380	228	0	804–868	927	0–20	4	7, 28, and 96	27–75
[26]	30	457	164.5	2.74	509–599	1303	0–15	3	1, 3, 7, and 28	10–58
Remarks	135	380–550	129–228	0–13.5	0–925	648–1303	0–100	1–40	1–96	5–76

Table 2
Summary of statistical analysis of input and target variables.

Statistical parameters	Input parameters								
	C	W	SP	FA	CA	R	MRS	T	CS
Mean	442.5	191.8	2.4	637.8	1003.6	17.1	5.3	23.8	36.8
SD	47.5	29.7	4.0	167.9	255.4	21.5	8.4	22.0	18.5
Var	2254.5	883.3	15.7	28198.4	65227.4	460.3	70.7	484.3	342.3
Kur	0.5807	−1.2322	3.6880	2.4050	2.7437	5.9103	12.745	5.242	−0.835
Skew	0.6660	−0.2165	2.2087	−1.0103	−1.2517	2.3979	3.666	2.187	0.253
Range	170	98.8	13.5	925	1303	100	40	95	70.8
Min	380	129.2	0	0	0	0	0	1	5
Max	550	228	13.5	925	1303	100	40	96	76
Count	135								

Cramer [9]. MEP is a type of genetic programming (GP) in which the chromosomes are presented linearly. Individuals in MEP are strings that encode complex computer programs into genes [10]. MEP permits storing multiple solutions in a single chromosome, which could be considered the main advantage of MEP over other techniques [11]. In MEP individuals, generally, several solutions are stored in each chromosome, then the best solution is selected. This is referred to as strongly understood parallelism and is a distinguishing feature of MEP [12,13]. Several fitting parameters are required to develop the MEP model, including the sub-population number and their size, code length, tournament size, and different mathematical operators. Trial and error are used to determine the training parameters of the MEP model [11].

2.2.2. Artificial neural network (ANN)

An artificial neural network simulates the human brain and processes data correspondingly [14–16]; it contains three layers: input, hidden, and output layer (Eq. (1)) [14]. These layers are connected through weights and biases; each node's output is transferred to other nodes through transfer functions. The current study developed the ANN model using a feed-forward back propagation neural network. The sigmoid activation function was used in the hidden layer, and linear activation was used in the output layer. Equation (2) shows the typical calculation of ANN output in a single node and illustrates the process displayed in Fig. 5.

$$\theta = \sum_{i=1}^{n} w_i \, x_i + bias \tag{1}$$

$$output = \frac{1}{1 + e^{-\theta}} \tag{2}$$

Where x and w are input variables and the weight related to that input, bias is the current node's bias.

2.2.3. Multi-Adaptive Regression Spline (MARS)

Friedman [17] introduced the MARS model, a nonparametric and nonlinear regression method. It is implemented using a collection of splines with changing gradients to represent the nonlinear interactions within an input and output system. The underlying substantial relationship between input-output variables does not need to be an ongoing assumption in this system. The nodes specify the start and end of one data region; respectively, they are the segment endpoints. The resulting splines (sometimes called base functions) allow the model more flexibility, thresholds, and other departures from linear functions. The implementation of MARS to build models follows a two-step process. In the first step (Forward Phase), the MARS starts the model development and starts with the intercept term, then repeatedly adds the basis function (BF) to reduce the sum of square error (residual error). In the second step (backward phase), the model is simplified, and unnecessary terms are removed to solve the overfitting problem and generalization of the model on new data [18]. Equation (3) shows the response function:
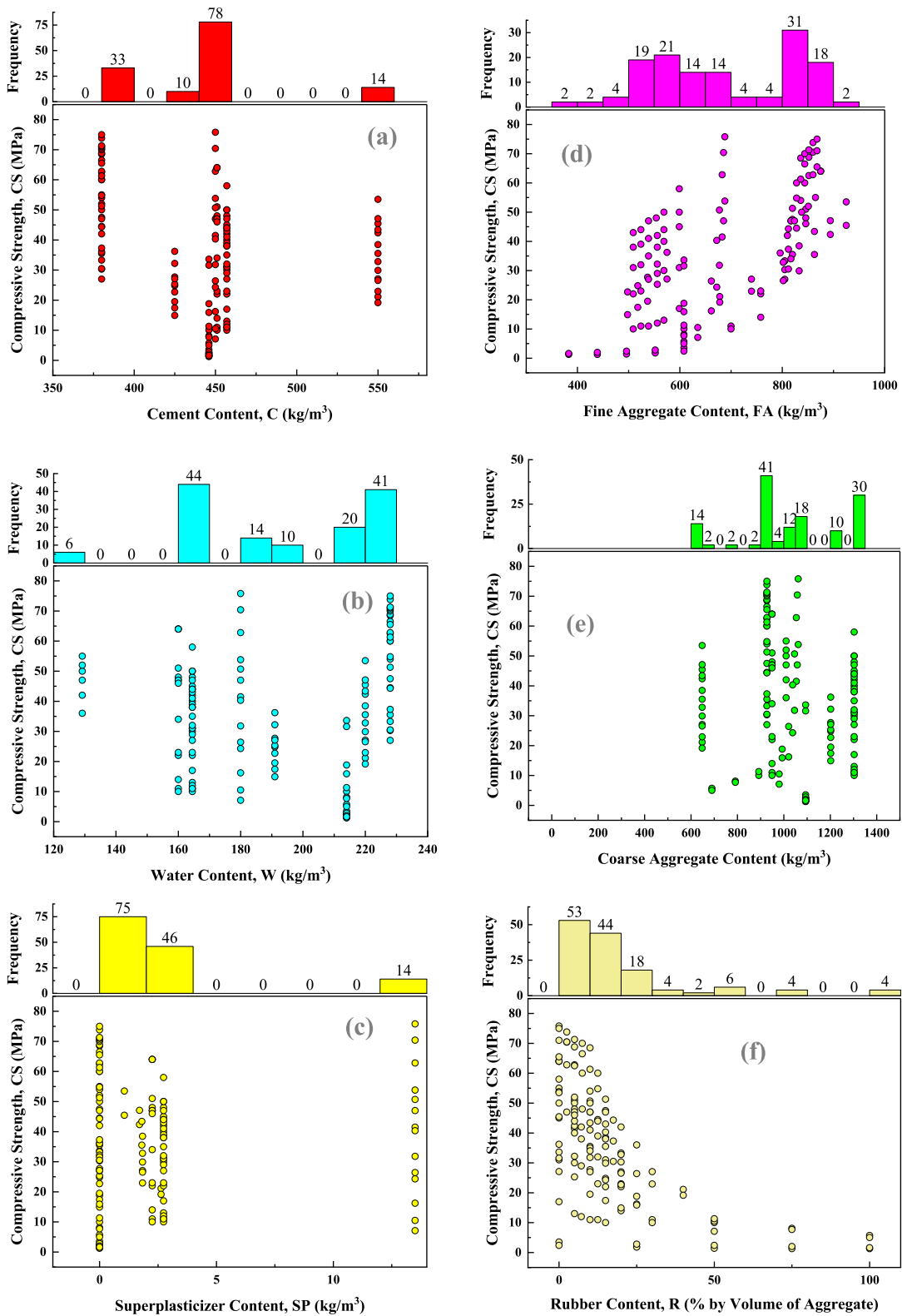
Fig. 2. Scatter plot with marginal histogram for the relation between CS and (a) cement content,(b) water content, (c) superplasticizer content, (d) fine aggregate content, (e) coarse aggregate content, (f) rubber content, (g) maximum rubber size, and (h) curing time.
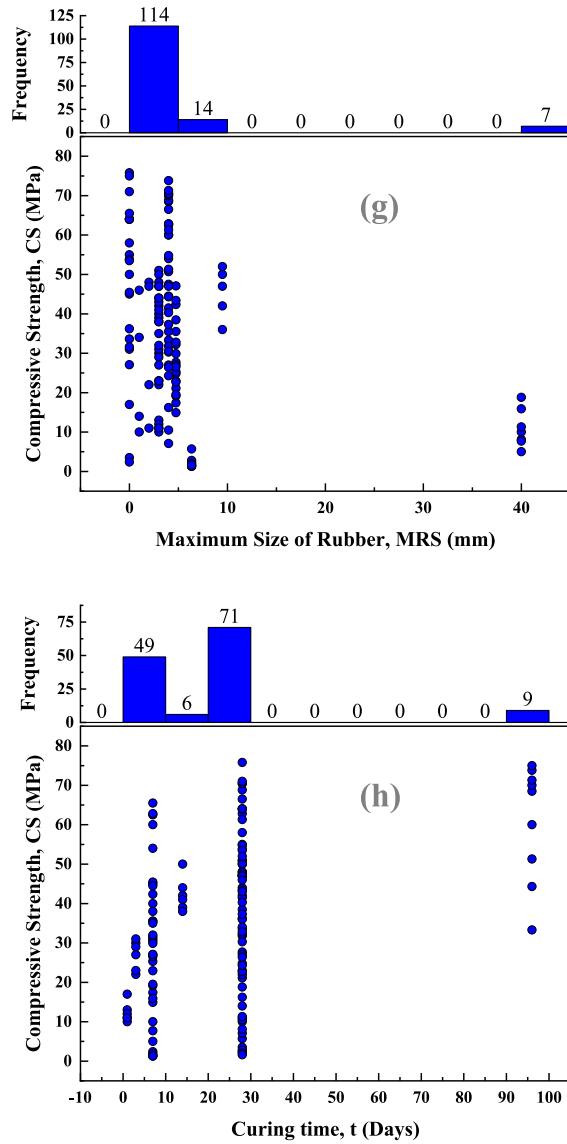
Fig. 2. (*continued*).

$$y = f(x1, \cdots, xn) + e \tag{3}$$

Where x, n, and e are the independent variables, n is the number of input variables, and the error value, respectively.

BFs are utilized in the MARS algorithm for approximating functions, which denotes the splines; there are two types of BFs, piecewise-linear and piecewise-cubic. Equation (4) shows the explanation of piecewise-linear, which was used in the current study to develop the MARS model:

$$BF = \max(0, x - t) \begin{cases} x - t & \text{if } x \geq t \\ 0 & \text{otherwise} \end{cases} \tag{4}$$

The MARS model linearly combines the BFs, which can be expressed as follows (Eq. (5)):

$$f(x) = \beta_0 + \sum_{k=1}^{N} \beta_k \gamma_k(x) \tag{5}$$

Where N is the total number of instances and β_o and β_k are the coefficients, $\gamma_k(x)$ also consists of one or more spline functions.
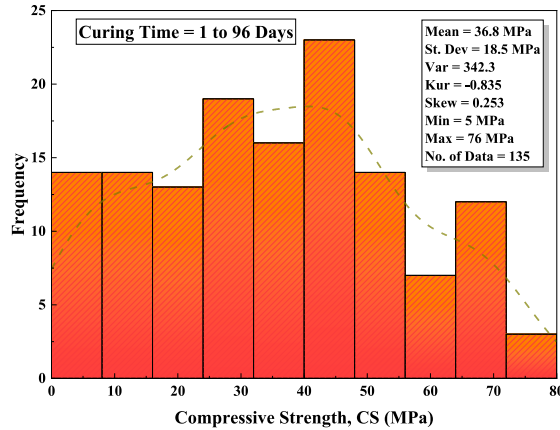
Fig. 3. Histogram for CS of rubberized concrete from 1 to 96 days of curing.
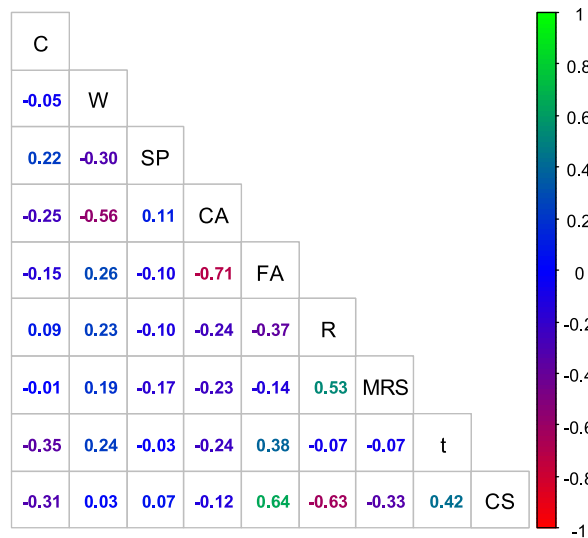
Fig. 4. Correlation matrix for target and predictors.

2.2.4. Nonlinear regression (NLR)

NLR is a type of multiple regression model; the model is developed using the solver technique and the least square method. The input variables are related to the target variable through model parameters and the power for each input. The model consists of two parts; in the first part, all the input parameters are used, and the result of part one is mathematically added to part two, which consists of only the input parameters in normal concrete like cement, water, fine aggregate, and coarse aggregate contents in addition to the curing time of the samples. Equation (6) shows the general form of the NLR model [19,20].

$$CS = \alpha_1 (C)^{\alpha_2} (W)^{\alpha_3} (SP)^{\alpha_4} (FA)^{\alpha_5} (CA)^{\alpha_6} (R)^{\alpha_7} (MRS)^{\alpha_8} (t)^{\alpha_9} + \alpha_{10} (C)^{\alpha_{11}} (W)^{\alpha_{12}} (FA)^{\alpha_{13}} (CA)^{\alpha_{14}} (t)^{\alpha_{15}} \qquad (6)$$

Where CS is the output of the NLR model, which is the compressive strength, α_1 to α_{15} are the model parameters.

2.3. Evaluation of the developed models

The developed models are compared and evaluated using the coefficient of determination (R^2), Root Mean Squared Error (RMSE), Scatter Index (SI), and Mean Absolute Percentage Error (MAPE). Those statistical parameters were used to determine the predictive models' performance; each tool's equation is presented in Eqs. (7)–(11). The Taylor diagram was also used to evaluate the performance of the predictive models.
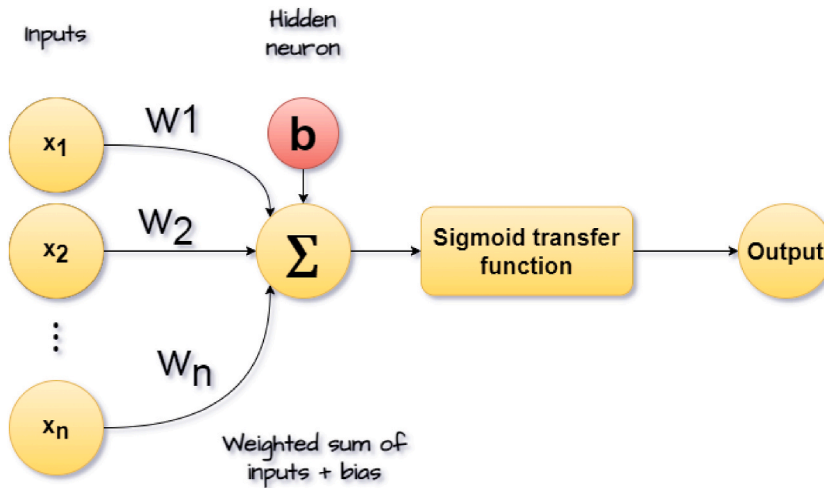
Fig. 5. Typical calculation of the ANN model.

$$R^2 = 1 - \frac{\sum_{i=1}^{n}(yp_i - yi)^2}{\sum_{i=1}^{n}(yi - \overline{yi})^2} \tag{7}$$

$$RMSE\ (MPa) = \sqrt{\frac{\sum_{i=1}^{n}(yp - yi)^2}{n}} \tag{8}$$

$$MAE\ (MPa) = \frac{\sum_{i=1}^{n}|yp - yi|}{n} \tag{9}$$

$$SI = \frac{RMSE}{\overline{ym}} \tag{10}$$

$$MAPE\ (\%) = \left|\frac{yp - ym}{ym}\right| \times 100 \tag{11}$$

Where yi or ym, yp, ($\overline{yi}$ or $\overline{ym}$) and n is measured compressive strength, predicted compressive strength, mean of measured compressive strength, and the total number of data in the related dataset. According to SI, the model performance is excellent, good, fair, and poor if the SI< 10%, 10% < SI<20%, 20% < SI<30%, and SI>30%, respectively [21].

3. Results and analysis

3.1. Developed MEP model

In the current study, an MEP model was created using the fitting parameters provided in Table 3; Trial and Error was used to

Table 3
Fitting parameters for the MEP model.

Fitting Parameter	Value
Subpopulation No.	10
Subpopulation Size	110
Code Length	300
Crossover Probability	1
Mutation Probability	0.01
Tournament Size	5
Functions and Variable Probability	0.5
Operators	+, -, *, and/
Generations	1000

Table 4
Detail about the MARS model.

Basis functions type	Piecewise-linear
Number of BFs (intercept is included)	35
Maximum interactions	12
MSE train (MPa)	10.2
MSE test (MPa)	18.9
Generalized cross-validation (GCV)	1.131e+03
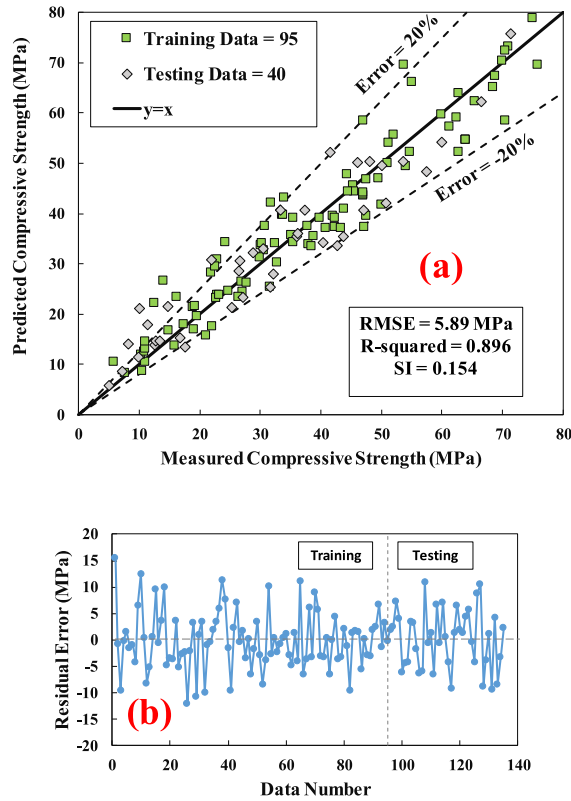
Fig. 6. Relationship between predicted CS using MEP model and measured CS (a) training dataset, (b) testing dataset, and (c) residual error between predicted and measured CS.

determine those parameters. Equation (12) shows the formula to calculate the CS of rubberized concrete using the MEP model. The scatter plot between actual (measured) and output (predicted) CS is shown in Fig. 6a. The R^2, RMSE, and SI are 0.914, 5.35 MPa, and 0.14 for the training dataset, 0.911, 5.5 MPa, and 0.166 for testing dataset. The calculated error between predicted and actual compressive strength is between −11 and 15 MPa (Fig. 6b) (see Table 4).

$$CS = \frac{\beta_1 - \beta_2 - \beta_3}{\beta_4} + \beta_5 - \beta_6 - \beta_7 \tag{12a}$$

$$\beta_1 = \left(g + \frac{d}{b}\right)\left(h + \frac{b+d+g}{b-c-f+g}\right) + \frac{d^2}{b} + b + g - c \tag{12b}$$

$$\beta_2 = -cf\left(h + \frac{b+d+g}{b-c-f+g}\right) - ec + b + g - c - f + \frac{eb}{d+bg-bc^2} \tag{12c}$$

$$\beta_3 = \frac{f(f-c)(b+g)(b-c-f+g)}{(b+g)(b+d+g) - e(b-c-f+g)} + d + f + h + \frac{b+d+g}{b-c-f+g} \tag{12d}$$

$$\beta_4 = 2a - 3b + cf + 3c + f - 3g \tag{12e}$$

$$\beta_5 = \frac{b(b-c-f+g)^2}{bg(b-c-f+g)+b(b+d+g)+d(b-c-f+g)} + \frac{\frac{d^2}{b}+a}{b+c^2-5c+2f+g} \tag{12f}$$

$$\beta_6 = \frac{\frac{b(b-c-f+g)^2}{bg(b-c-f+g)+b(b+d+g)+d(b-c-f+g)} + \frac{\frac{d^2}{b}+a}{b+c^2-5c+2f+g}}{h} \tag{12g}$$

$$\beta_7 = \left(\frac{a + \left(g+\frac{d}{b}\right)*\left(\frac{b+g+d}{b+g-c-f}+h\right)}{e*c + \left(g+\frac{d}{b}\right)*\left(\frac{b+g+d}{b+g-c-f}+h\right)} \right) \tag{12h}$$

3.2. Developed ANN model

In this study, an ANN model structure was constructed, as shown in Fig. 7. In addition to input and output layers, two hidden layers were included. Equation (13) can be used to determine the compressive strength of rubberized concrete using the ANN model. The R^2, RMSE, and SI are 0.914, 5.35 MPa, 0.14 for the training dataset, 0.911, 5.5 MPa, and 0.166 for the testing dataset, as shown in Fig. 8a. The residual error between predicted and measured CS was changed from −13 to 12 MPa (Fig. 8b). The required weight and bias values to calculate CS are provided in the following matrices.

$$\begin{vmatrix} -6.997 & 4.311 & 5.094 & 3.228 & -2.615 & 0.505 & 1.323 & -13.484 & -4.755 \\ -37.036 & 16.773 & 30.491 & 8.880 & -29.160 & 5.859 & 2.101 & -32.642 & 21.163 \\ 0.284 & 1.089 & 0.428 & 3.053 & 3.579 & 0.122 & 0.296 & 0.393 & -4.703 \end{vmatrix} \times \begin{vmatrix} C \\ W \\ SP \\ FA \\ CA \\ R \\ MRS \\ t \\ 1 \end{vmatrix} = \begin{vmatrix} \beta_1 \\ \beta_2 \\ \beta_3 \end{vmatrix}$$

$$\begin{vmatrix} node1 & node2 & node3 & -4.476 \end{vmatrix} \times \begin{vmatrix} 10.427 \\ -12.518 \\ 1.631 \\ 1 \end{vmatrix} = \begin{vmatrix} \beta_4 \end{vmatrix}$$

$$\begin{vmatrix} node1 & node2 & node3 & 7.572 \end{vmatrix} \times \begin{vmatrix} 3.603 \\ -7.442 \\ -22.277 \\ 1 \end{vmatrix} = \begin{vmatrix} \beta_5 \end{vmatrix}$$

$$\begin{vmatrix} node1 & node2 & node3 & -1.258 \end{vmatrix} \times \begin{vmatrix} -3.786 \\ -27.198 \\ 17.056 \\ 1 \end{vmatrix} = \begin{vmatrix} \beta_6 \end{vmatrix}$$

$$CS = \frac{0.863}{1+e^{-\beta_4}} - \frac{1.84}{1+e^{-\beta_5}} + \frac{1.354}{1+e^{-\beta_6}} + 0.901 \tag{13}$$

3.3. Developed MARS model

Equation (14) is the formula for the MARS model. Fig. 9a shows a scatter plot between rubberized concrete's actual (measured) and output (predicted) CS. The R^2, RMSE, and SI are 0.969, 3.19 MPa, and 0.083 for the training dataset, 0.945, 4.35 MPa, and 0.131 for the testing dataset. The BFs from 1 to 34 can be obtained from Table 5. The residual error in training and testing datasets was between −15 and 13 MPa (Fig. 9b).
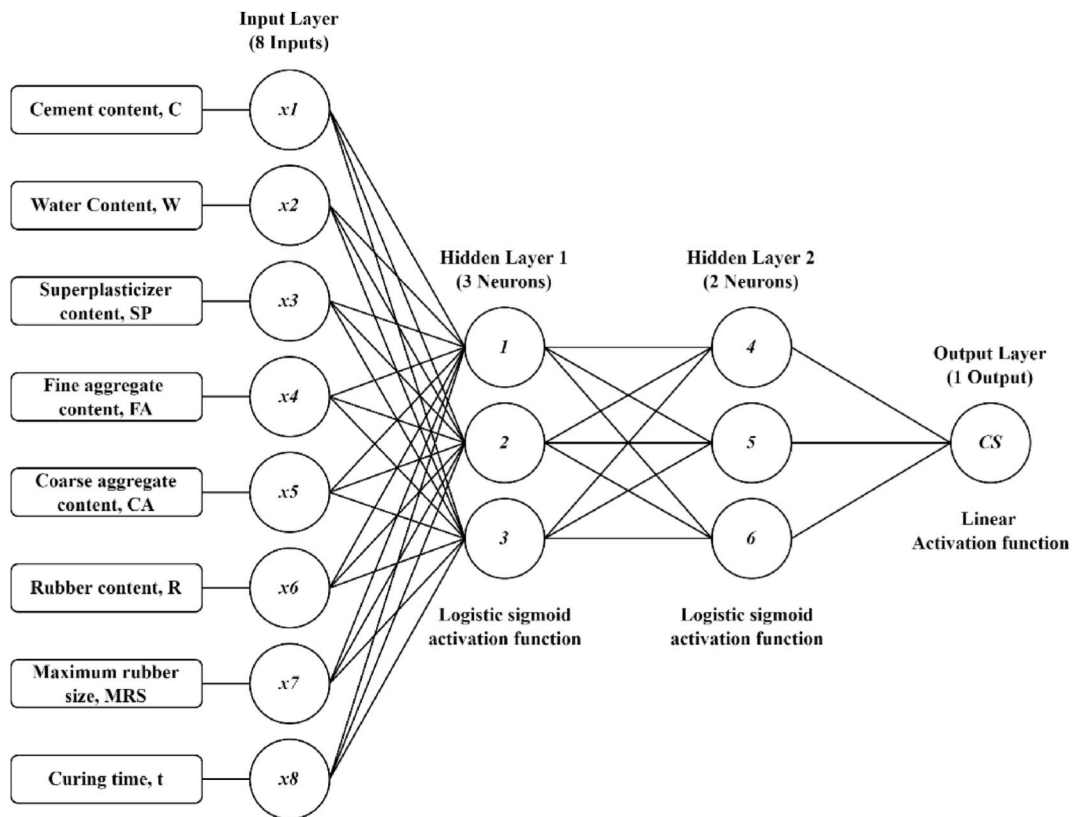
Fig. 7. Selected ANN structure.
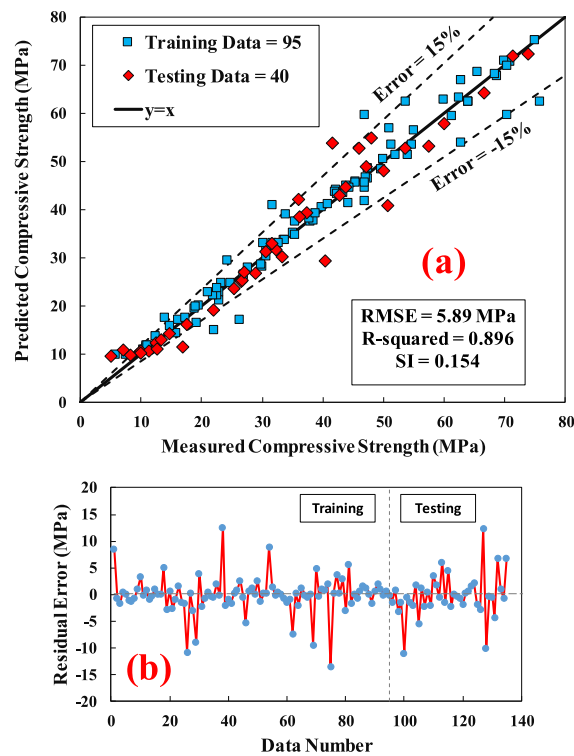
Fig. 8. Relationship between predicted CS using ANN model and measured CS (a) training dataset, (b) testing dataset, and (c) residual error between predicted and measured CS.
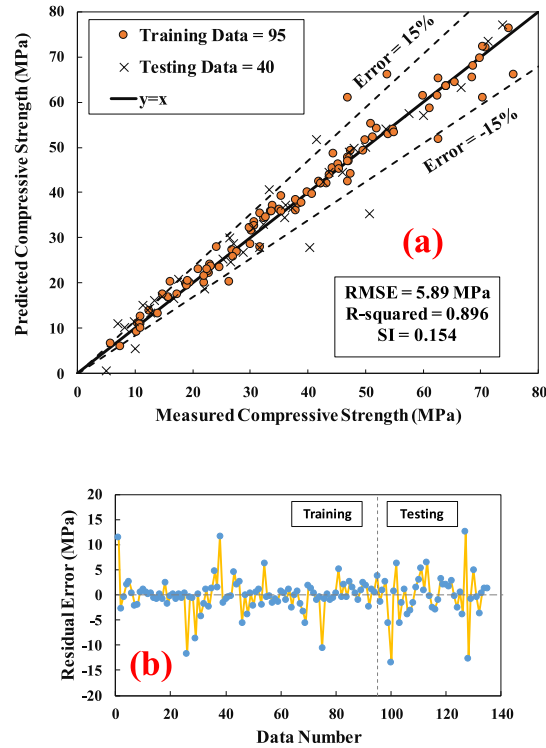
Fig. 9. Relationship between predicted CS using MARS model and measured CS (a) training dataset, (b) testing dataset, and (c) residual error between predicted and measured CS.

Table 5
Related basis functions for the MARS model.

BF	Function
BF1	max(0, R - 25)
BF2	max(0,25 - R)
BF3	BF2 * max(0, FA - 760)
BF4	BF2 * max(0,760 - FA)
BF5	max(0, t - 7)
BF6	max(0,7 - t)
BF7	BF4 * max(0, W - 160)
BF8	BF4 * max(0,160 - W)
BF9	BF4 * max(0, W - 164.5)
BF10	BF4 * max(0,164.5 - W)
BF11	BF3 * max(0, C - 457)
BF12	BF3 * max(0,457 - C)
BF13	BF5 * max(0, CA - 1010)
BF14	BF5 * max(0,1010 - CA)
BF15	BF5 * max(0, W - 180)
BF16	BF5 * max(0,180 - W)
BF17	max(0, SP - 1.81)
BF18	max(0,1.81 - SP)
BF19	BF2 * max(0, W - 220)
BF20	BF2 * max(0,220 - W)
BF21	BF2 * max(0, CA - 1038)
BF22	BF2 * max(0,1038 - CA)
BF23	max(0, FA - 619.2)
BF24	max(0,619.2 - FA)
BF25	max(0, MRS - 4)
BF26	max(0,4 - MRS)
BF27	max(0, R - 2.5)
BF28	max(0,2.5 - R)
BF29	BF24 × max(0, SP - 2.74)

(*continued on next page*)

Table 5 (*continued*)

BF	Function
BF30	BF24 × max(0,2.74 - SP)
BF31	BF2 * max(0, t - 28)
BF32	BF2 * max(0,28 - t)
BF33	max(0, t - 3)
BF34	max(0,3 - t)

$$
\begin{aligned}
CS = {} & -78.9 - 4.48^*BF1 + 7.65^*BF2 + 0.0002^*BF3 + 0.0256^*BF4 + 0.111^*BF5 - 2.77^*BF6 - 0.00^*BF7 + 0.0131^*BF8 \\
& + 0.00571^*BF9 - 0.0119^*BF10 + 0.0007^*BF13 + 0.0001^*BF14 + 0.0018^*BF15 + 0.00856^*BF16 + 0.341^*BF17 + 0.496^*BF18 \\
& - 0.208^*BF19 - 0.0424^*BF20 + 0.0023^*BF21 - 0.0141^*BF22 + 0.219^*BF23 + 0.0892^*BF24 - 0.0316^*BF25 - 5.35^*BF26 \\
& + 4.26^*BF27 + 2.43^*BF28 - 0.0102^*BF29 - 0.0275^*BF30 - 0.004^*BF31 - 0.008^*BF32 - 0.0491^*BF33 - 3.28^*BF34
\end{aligned}
$$

$$(14)$$

3.4. Developed NLR model

The developed NLR model formula is shown in Eq. (15). The solver technique calculates the model parameters, the summation of the square errors (SSE) is calculated, and the target of the solver is SSE minimum value; the model training was completed when the minimum SSE reached, according to the result the formula of NLR model is updated. The problem of zero content of some of the input parameters was solved by adding a small amount (i.e., 0.001) to all the input values with zero; for example, 0.001 should be added to the rubber content in the model since it has zero values. The scatter plot between predicted values using the NLR model and the actual compressive strength is shown in Fig. 10 a; the R^2, RMSE, and SI are 0.896, 5.89, and 0.154 for training and 0.877, 6.65, and 0.201 for testing dataset. Fig. 10b shows the residual error for the NLR model, ranging from −19 to 14 MPa.
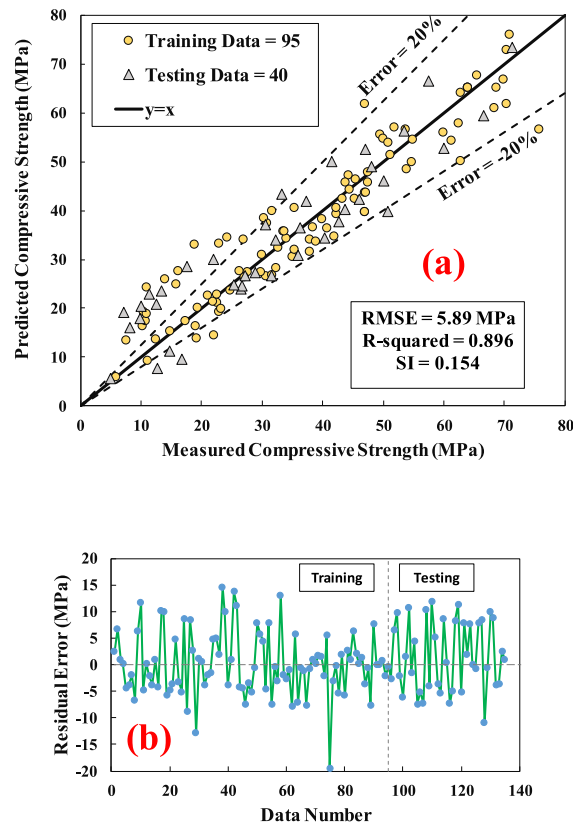
Fig. 10. Relationship between predicted CS using NLR model and measured CS (a) training dataset, (b) testing dataset, and (c) residual error between predicted and measured CS.

$$CS = \frac{6.87 \times (C)^{3.081} \times (SP)^{0.035} \times (CA)^{0.810} \times (MRS)^{0.337} \times (t)^{0.284}}{10^7 \times (W)^{1.416} \times (FA)^{0.025} \times (R)^{0.340}} + \frac{0.021 \times (W)^{1.638} \times (FA)^{3.180} \times (CA)^{0.040} \times (t)^{0.052}}{(C)^{3.846}} \tag{15}$$
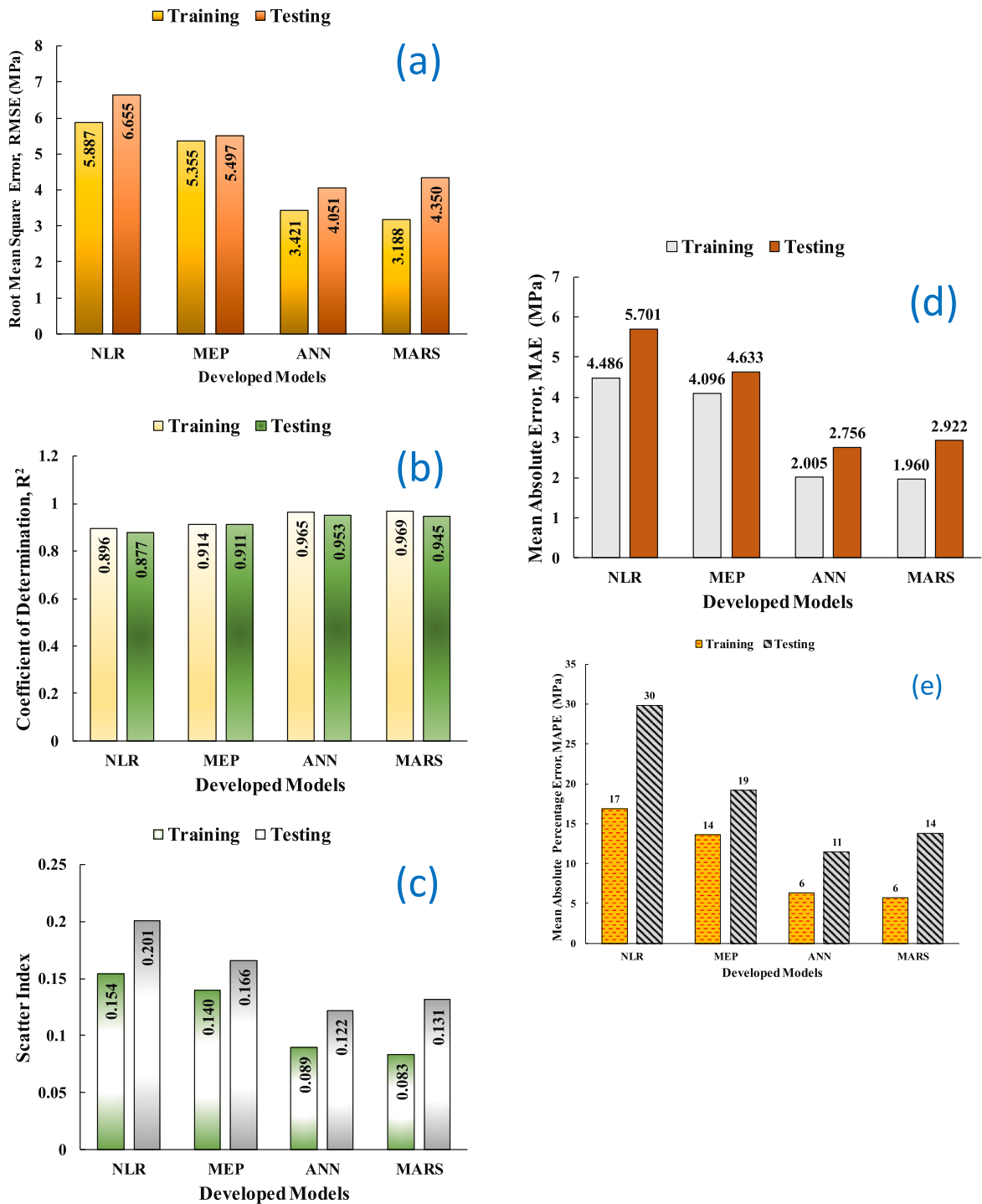
Fig. 11. Performance of the created models based on (a) RMSE, (b) R^2, (c) SI, (d) MAE, and (e) MAPE.

3.5. Comparison between the performance of the developed models

The performance of the developed models is compared based on the mentioned assessment tools, as shown in Figs. 11 and 12. The performance of the ANN model according to RMSE and R^2 (Fig. 11a and b) is better than other models since the RMSE of the ANN model is 3.421 and 4.051 MPa in the training and testing datasets with higher R^2, respectively, except that the RMSE of MARS model in the training dataset is smaller. Similarly, the coefficient of determination of the MARS model in the training dataset is larger than in other models; however, the R^2 of the ANN model in the testing dataset is smaller. It can also be obtained in Fig. 11c and d, the ANN model outperforms other developed models in the testing dataset since the scatter plot and MAE of the ANN model are smaller than MEP, MARS, and NLR models.

Additionally, the MAPE of the ANN model (Fig. 11e) in training and testing datasets are 6 and 11%; for the MARS model, the MAPE values are 6 and 14% in training and testing datasets here, the result shows that the prediction of the ANN model has less error in the testing dataset than MARS model which was 3% less error on the unseen data. Fig. 12 (a, b) shows the Taylor diagram for comparing the developed models; as shown for the training dataset, ANN and MARS models are performed nearly the same, and it is also clear the ANN model is the best in the testing dataset. The comparison between developed models based on scatter plot between measured and predicted CS of the testing dataset is shown in Fig. 13; the figure indicated that the ANN model has less scatter and almost all the points (predicted-measured relationship) are located between 20 and −20% error lines.

3.6. Performance of the proposed models in predicting CS of different sample sizes

The collected data contained three different sizes: S1 is a 150 × 300 mm cylinder, S2 is 150 × 150 × 150 mm cubes, and S3 is a 100 × 200 mm cylinder. The total number for each size in the training and testing data set is shown in Fig. 14. The prediction of the developed models for all the data is calculated, as mentioned before. Moreover, the developed model's performance in predicting the CS of rubberized concrete for different sample sizes is also determined using the Correlation Coefficient (R) and RMSE. As summarized
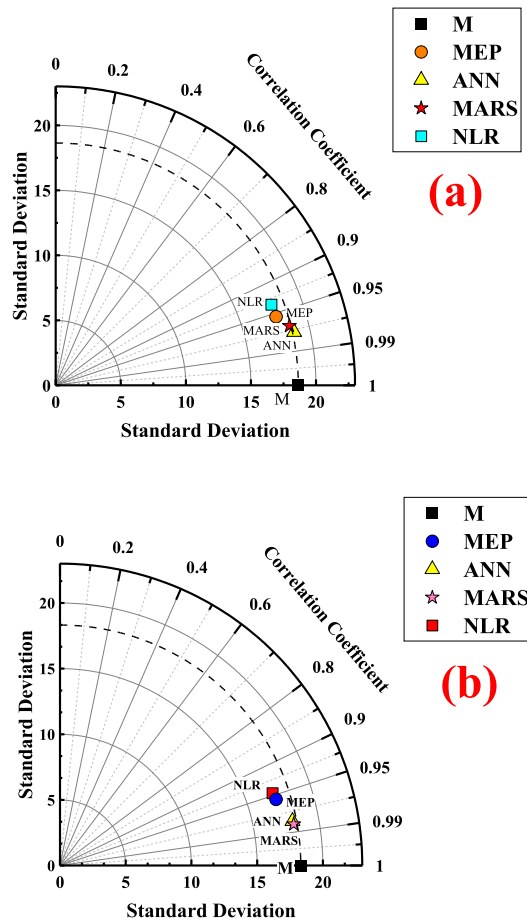
Fig. 12. Comparison between developed models based on standard deviation and the correlation coefficient between measured and predicted CS (a) training dataset and (b) testing dataset.
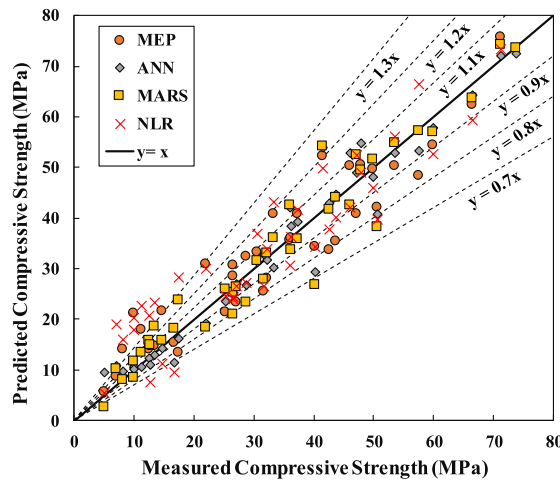
Fig. 13. Comparison between developed models based on scatter plot between measured and predicted CS of the testing dataset.
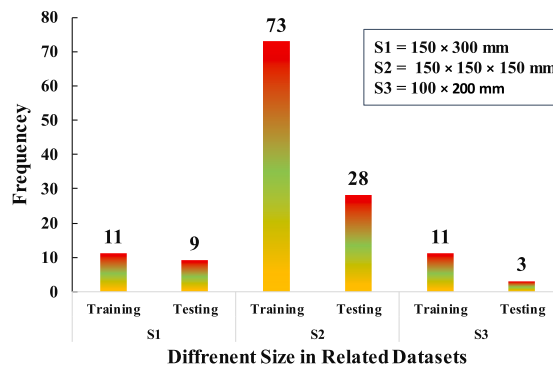
Fig. 14. Number of data for different sizes in training and testing datasets.

in Table 6, ANN and MARS models predicted the CS of rubberized concrete for all sizes better than MEP and NLR models with high R and low RMSE.

3.7. Effect of the maximum size of rubber on the compressive strength of rubberized concrete

To determine the effect of the maximum size of rubber on compressive strength, the best model, which ANN model, was used, and a mixture was decided based on the mean of collected datasets. Two databases were constructed in the first on the fine aggregate replaced by rubber, and the maximum size changed from 1 to 4.75 mm; in the second on the coarse aggregate replaced by rubber, the maximum size changed from 9.5 to 25 mm. The result of this parametric test using the ANN model is shown in Fig. 15a and b. The result indicated that when the maximum size of rubber increased, the compressive strength loss was also increased; a similar result was

Table 6
Summary of the performance of the developed models in predicting the CS of rubberized concrete using a different sample size.

Sample size	Dataset	No. of Data	R				RMSE (MPa)				
			NLR	MEP	ANN	MARS	NLR	MEP	ANN	MARS	Best Model Performance
S1 (150 × 300 mm)	Training	11	0.795	0.922	0.955	0.989	6.4	4.0	2.8	1.4	MARS
	Testing	9	0.529	0.837	0.934	0.953	7.0	4.4	2.6	2.3	MARS
S2 (150 × 150 × 150 mm)	Training	73	0.944	0.951	0.979	0.982	6.2	5.7	3.7	3.5	MARS
	Testing	28	0.923	0.940	0.965	0.954	6.8	5.9	4.6	5.2	ANN
S3 (100 × 200 mm)	Training	11	0.964	0.940	0.993	0.985	2.8	3.8	1.1	1.7	ANN
	Testing	3	0.993	0.975	0.995	0.988	3.5	4.2	1.3	3.3	ANN
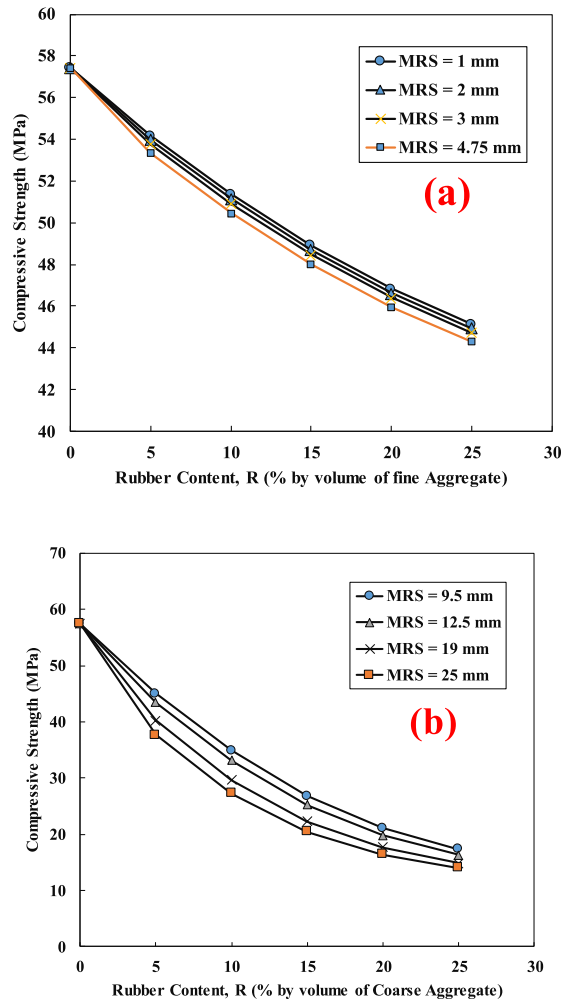
Fig. 15. Effect of the maximum size of rubber on the compressive strength of rubberized concrete up to 25% of rubber replaced (a) fine aggregate and (b) coarse aggregate.

obtained by Abbas et al. [22] when the aggregate was replaced by rubber with a maximum size of 1, 5, and 10 mm. The compressive strength loss in the mixes with coarse aggregate replaced by rubber is higher than in fine aggregate replacement [1,22].
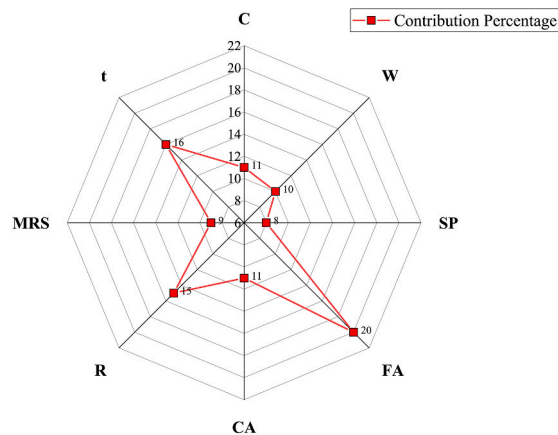
Fig. 16. Radar plot for contribution percentage of input parameters in rubberized concrete CS prediction.

3.8. Contribution percentage of input parameter in predicting CS of rubberized concrete

Fig. 16 shows the contribution percentage of predictors (input parameters) in the rubberized concrete CS prediction; the MEP model was used in the determination process. The model was trained several times; each time a single predictor was removed from the training dataset. After training, the error was measured, which was the mean square error (MSE). Finally, from the sensitivity of the model against each input, the contribution percentages were determined. The result suggested that the FA affects the compressive strength of rubberized more than other input parameters since the contribution parameter is greater than the curing time and rubber content; furthermore, the less effective parameter is superplasticizer content.

4. Conclusions

In the current study, the compressive strength of rubberized concrete was predicted using four distinct modeling approaches; 135 datasets were collected from previous literature, then the statistical analysis was performed on the collected data. After that, the collected data were divided randomly and used in the model development. The following points are concluded from the result of the current study.

1. Increasing the rubber content decreases the compressive strength of concrete since the density of rubber is less than that of natural aggregate.
2. Replacing natural aggregate with waste rubber causes a decrease in the unit weight of the concrete mixture.
3. Per performance measure criteria, the ANN model has high R^2 with low RMSE, MAE, SI, and MAPE.
4. Based on the Taylor diagram, the ANN model performed better than MARS, MEP, and NLR models.
5. The NLR model formula is simpler than ANN, MARS, and MEP models and requires less training time. However, the performance of the NLR model in the training and testing datasets is poor.
6. ANN and MARS models predicted the CS of rubberized concrete with different sample sizes better than MEP and NLR models, with low RMSE and high R.
7. Parametric analysis suggests that the compressive strength loss increases with increasing maximum rubber size, and the strength loss in the coarse aggregate replacement is higher than in fine aggregate replacement.
8. Fine aggregate content is the most effective parameter on the compressive strength of rubberized concrete since it contributes to the prediction of CS more than other input parameters than the curing time of the concrete samples.

Availability of data and materials

The data supporting the conclusions of this article are included in the article.

Funding

Ethics approval and consent to participate

Not applicable.

CRediT authorship contribution statement

Dilshad Kakasor Ismael Jaf: Conceptualization, Data curation. **Aso Abdalla:** Funding acquisition. **Ahmed Salih Mohammed:** Investigation. **Payam Ismael Abdulrahman:** Methodology. **Rawaz Kurda:** Conceptualization. **Azad A. Mohammed:** Writing – review & editing.

Declaration of competing interest

The author declares that they have no known competing financial interests or personal relationships that could have appeared to influence the work reported in this paper.

References

[1] N.N. Eldin, A.B. Senouci, Measurement and prediction of the strength of rubberized concrete, Cement Concr. Compos. 16 (4) (1994) 287–298.
[2] E. Güneyisi, M. Gesoğlu, T. Özturan, Properties of rubberized concretes containing silica fume, Cement Concr. Res. 34 (12) (2004) 2309–2317.
[3] H. Antil, M. Heinkenschloss, D.C. Sorensen, Application of the Discrete Empirical Interpolation Method to Reduced Order Modeling of Nonlinear and Parametric Systems. Reduced Order Methods for Modeling and Computational Reduction, 2014, pp. 101–136.
[4] M. Nehdi, A. Khan, Cementitious composites containing recycled tire rubber: an overview of engineering properties and potential applications, Cem. Concr. Aggregates 23 (1) (2001) 3–10.
[5] A. Grinys, H. Sivilevičius, M. Daukšys, Tyre rubber additive effect on concrete mixture strength, J. Civ. Eng. Manag. 18 (3) (2012) 393–401.

[6] I.G. Shaaban, J.P. Rizzuto, A. El-Nemr, L. Bohan, H. Ahmed, H. Tindyebwa, Mechanical properties and air permeability of concrete containing waste tires extracts, J. Mater. Civ. Eng. 33 (2) (2021) 04020472.

[7] M. Kovačević, S. Lozančić, E.K. Nyarko, M. Hadzima-Nyarko, Modeling of compressive strength of self-compacting rubberized concrete using machine learning, Materials 14 (15) (2021) 4346.

[8] D. Yin, H. Jin, X. Gu, S. Yu, Z. Wang, Influence of rubber geometrical characteristics on the corrosion behavior of rebar in rubberized concrete, J. Build. Eng. (2023) 107535.

[9] Y. Jiang, S. Zhang, G. Xue, W. Wang, Compressive behavior of rubberized concrete under high strain rates, Structures 56 (2023, October) 104983. Elsevier.

[10] X. Gao, J. Yang, H. Zhu, J. Xu, Estimation of rubberized concrete frost resistance using machine learning techniques, Construct. Build. Mater. 371 (2023) 130778.

[11] Osama Youssf, M.A. Elgawady, An Overview of Sustainable Concrete Made with Scrap Rubber, 2012, pp. 1039–1044.

[12] R. Roychand, R.J. Gravina, Y. Zhuge, X. Ma, J.E. Mills, O. Youssf, Practical rubber pre-treatment approach for concrete use—an experimental study, Journal of Composites Science 5 (6) (2021) 143.

[13] O. Youssf, M.A. ElGawady, J.E. Mills, X. Ma, Analytical modeling of the main characteristics of crumb rubber concrete, ACI Spec. Publ. 314 (2017) 1–18.

[14] O. Youssf, R. Hassanli, J.E. Mills, Y. Zhuge, Axial compression behaviour of hybrid double-skin tubular columns filled with rubcrete, Journal of Composites Science 3 (2) (2019) 62.

[15] Singh, P., Bhardwaj, S., Dixit, S., Shaw, R.N., and Ghosh, A., Development of Prediction Models to Determine Compressive Strength and Workability of Sustainable Concrete with ANN. Springer.

[16] P.G. Asteris, A. Ashrafian, M. Rezaie-Balf, Prediction of the compressive strength of self-compacting concrete using surrogate models, Comput. Concr. 24 (2) (2019) 137–150.

[17] P.G. Asteris, S. Nozhati, M. Nikoo, L. Cavaleri, M. Nikoo, Krill herd algorithm-based neural network in structural seismic reliability evaluation, Mech. Adv. Mater. Struct. 26 (13) (2019) 1146–1153.

[18] P.G. Asteris, M.E. Lemonis, T.-T. Le, K.D. Tsavdaridis, Evaluation of the ultimate eccentric load of rectangular CFSTs using advanced neural network modeling, Eng. Struct. 248 (2021) 113297, https://doi.org/10.1016/j.engstruct.2021.113297.

[19] P.G. Asteris, P.B. Lourenço, M. Hajihassani, C.-E.N. Adami, M.E. Lemonis, A.D. Skentou, R. Marques, H. Nguyen, H. Rodrigues, H. Varum, Soft computing based models for the prediction of masonry compressive strength, Eng. Struct. 248 (2021) 113276, https://doi.org/10.1016/j.engstruct.2021.113276.

[20] I. Rahimi, A.H. Gandomi, P.G. Asteris, F. Chen, Analysis and prediction of covid-19 using sir, seiqr and machine learning models: Australia, Italy and UK cases, Information 12 (3) (2021) 1–25, https://doi.org/10.3390/info12030109, 109.

[21] L. Burhan, K. Ghafor, A. Mohammed, Modeling the effect of silica fume on the compressive, tensile strengths and durability of NSC and HSC in various strength ranges, Journal of Building Pathology and Rehabilitation 4 (2019) 1–19.

[22] A. Bardhan, R. Biswas, N. Kardani, M. Iqbal, P. Samui, M.P. Singh, P.G. Asteris, A novel integrated approach of augmented grey wolf optimizer and ANN for estimating axial load carrying-capacity of concrete-filled steel tube columns, Construct. Build. Mater. 337 (2022) 127454.

[23] P.G. Asteris, P.B. Lourenço, M. Hajihassani, C.-E.N. Adami, M.E. Lemonis, A.D. Skentou, R. Marques, H. Nguyen, H. Rodrigues, H. Varum, Soft computing based models for the prediction of masonry compressive strength, Eng. Struct. 248 (2021) 113276, https://doi.org/10.1016/j.engstruct.2021.113276.

[24] H. Zhang, H. Nguyen, X.N. Bui, et al., A generalized artificial intelligence model for estimating the friction angle of clays in evaluating slope stability using a deep neural network and Harris Hawks optimization algorithm, Eng. Comput. 38 (Suppl 5) (2022) 3901–3914, https://doi.org/10.1007/s00366-020-01272-9.

[25] C. Vipulanandan, A. Mohammed, R.G. Samuel, Smart bentonite drilling muds modified with iron oxide nanoparticles and characterized based on the electrical resistivity and rheological properties with varying magnetic field strengths and temperatures, in: Offshore Technology Conference, OTC, 2017, May D041S045R005.

[26] C. Vipulanandan, R. Krishnamoorti, A. Mohammed, V. Boncan, G. Narvaez, B. Head, J.M. Pappas, Iron nanoparticle modified smart cement for real time monitoring of ultra deepwater oil well cementing applications, in: Offshore Technology Conference, OTC, 2015, May OTC-25842;

[26] P.G. Asteris, M. Koopialipoor, D.J. Armaghani, E.A. Kotsonis, P.B. Lourenço, Prediction of cement-based mortars compressive strength using machine learning techniques, Neural Comput. Appl. 33 (19) (2021) 13089–13121, https://doi.org/10.1007/s00521-021-06004-8.